ADVANCED MATERIALS
www.advmat.de

# Hypergap Optical Materials

*Xiaolei Hu, Xiang Guo, Zhengran Wu, Kun Chen, Xintian Chen, Zhilin Li, and Ling Lu**

**Optical materials primarily refer to transparent insulators and semiconductors for guiding, diffracting, and nonlinearly-generating light at photon energies below the electronic bandgaps. This work proposes that a solid can be equally lossless, above the fundamental bandgap, in an energy interval dubbed the hypergap, when the conduction and valence bands are well-isolated. The optics within the hypergap could defy the conventional rules and limits set by the bandgap materials, including the low-loss negative permittivity unavailable in existing metals, the anomalous-dispersion phase matching in crystals without birefringence or microstructures, as well as the negative group-velocity dispersion across the visible spectrum unattainable in known dielectrics. High-throughput searches are performed in comprehensive material databases, predict over a hundred hypergap candidates, and experimentally verify one of them. Therefore, hypergap materials might lead to lower loss plasmonic metamaterials, easier wavelength converters in nonlinear optics, and simpler pulse stretchers or compressors in ultrafast optics, potentially transforming optics with unexplored material opportunities.**

## 1. Introduction

Bandgap materials, from glasses in lenses and fibers to semiconductors in integrated photonics, form the backbone of optics,[1–4] because the electronic bandgap is currently the only known mechanism allowing a solid to be effectively lossless at the optical frequencies, below the bandgap and above the infrared phonon absorption. However, the bandgap also imposes significant constraints on the optical responses of materials and eventually limits the functionalities of all optical components and devices. These fundamental constraints are from the normal material dispersions dominated by the interband electronic transitions above the bandgap. One constraint is the normal (phase-velocity) dispersion: the refractive index monotonically increases with frequency in the bandgap. Consequently, the dielectric constant is always greater than unity, the vacuum value, in lossless media; one is left with no choice but to use the lossy metals for their negative permittivities in plasmonics and metamaterials.[5,6] The normal (phase-velocity) dispersion also removes the possibility of phase matching at different wavelengths in isotropic materials for nonlinear[7,8] optics. The other constraint is the normal group-velocity dispersion (positive GVD): the group velocity monotonically decreases with frequency in the bandgap at the visible wavelengths. In order to compensate for the pulse distortions due to the positive material GVD, the negative GVD has to be produced using intricate geometric designs in ultrafast optics.[9,10]

In this work, we propose that a solid can possess a new lossless optical window, dubbed the hypergap, above the fundamental bandgap, in which the aforementioned optical constraints in the bandgap can be eliminated. As illustrated in **Figure 1**, the hypergap opens when the conduction and valence bands are sufficiently isolated from the rest electronic states, so that the photon absorption vanishes not only in the bandgap but also in the hypergap. Since the bandgap and the hypergap locate on the opposite sides of the electronic interband absorption, the dispersion relations within the two lossless gaps can be drastically distinct. Here, we highlight three remarkable optical properties of the hypergap materials and their potential applications.

First, the hypergap could offer ultra-low-loss negative permittivity — the elusive holy grail of plasmonics and metamaterials.[11,12] Shown in Figure 1b, the dielectric constant can be negative in the hypergap, due to the anomalous dispersion within the interband absorption, where the permittivity decreases with frequency. Previously, lossless negative permittivity was proposed in hypothetical lossless metals.[13] However, the high-throughput search[14,15] indicates that a narrow-band metallic state is generally unstable energetically and is hard to predict theoretically. In contrast, the hypergap material proposed in this work has an insulating ground state and is thus much more consistent with the ab-initio results. As a result, negative-epsilon hypergap insulator is a new direction for overcoming the ohmic loss in plasmonics.

Second, the hypergap enables the anomalous-dispersion phase matching – permitting even the isotropic or amorphous bulk materials for efficient nonlinear optical processes. Phase matching is the key requirement for frequency conversion and entangled-photon generation, while the current nonlinear

X. Hu, X. Guo, Z. Wu, K. Chen, X. Chen, Z. Li, L. Lu
Institute of Physics
Chinese Academy of Sciences/Beijing National Laboratory for Condensed Matter Physics
Beijing 100190, China
E-mail: linglu@iphy.ac.cn
X. Hu, X. Guo, Z. Wu, K. Chen, X. Chen
School of Physical Sciences
University of Chinese Academy of Sciences
Beijing 100049, China

The ORCID identification number(s) for the author(s) of this article can be found under https://doi.org/10.1002/adma.202512769

**DOI: 10.1002/adma.202512769**

 

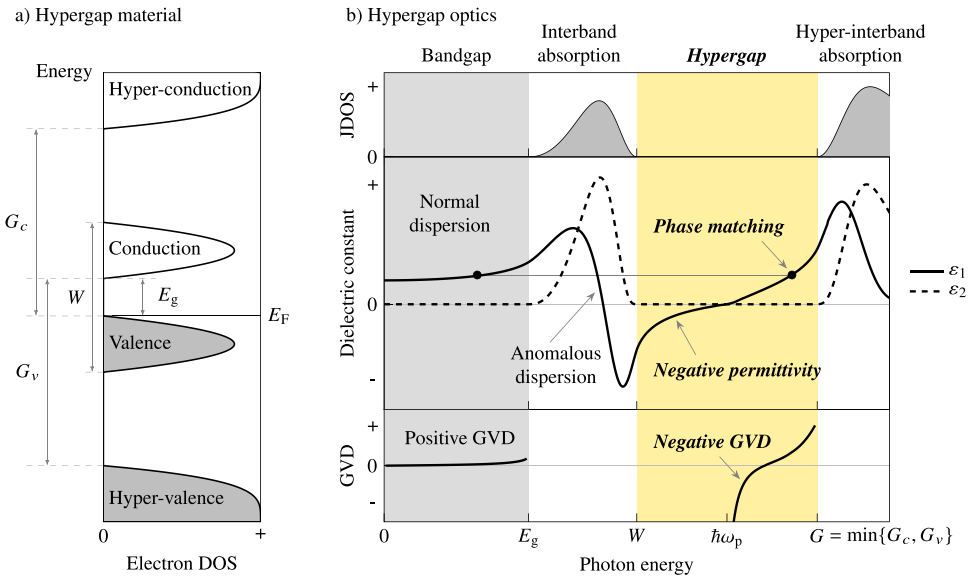


**Figure 1.** Hypergap material for optics. a) The electronic states of the hypergap material, where $E_g$ is the bandgap. b), Conceptual illustration of the momentum-relaxed joint density of states (JDOS), dielectric constants, and group-velocity dispersions (GVD) of the hypergap material. The refractive index $n = \sqrt{\epsilon_1}$ when $\epsilon_2 = 0$. The low-energy phonon absorption in the infrared is not illustrated in the plot.

crystals are either highly-anisotropic or periodically-poled in order to phase-match through birefringence or quasi-momentum. None of these conditions are needed for an anomalous-dispersion phase-matched hypergap material, in which the refractive index in the bandgap equals that in the hypergap (Figure 1b). In the past, anomalous-dispersion phase matching was explored by doping various hosting materials.[16–19] An intrinsically phase-matched hypergap material could enable more convenient approaches for nonlinear light generation.

Third, the hypergap introduces negative (anomalous) GVD at optical wavelengths (<1μm), unattainable in normal materials[9] but absolutely indispensable in ultrafast optics. Due to the lack of negative material GVD, effective negative GVDs from angular dispersions[20] (using grating pairs[21] and prism pairs)[22] are ubiquitously used to compensate the positive material GVDs in order to maintain short pulses in the system. The negative GVD is also crucial for soliton formation by balancing the Kerr nonlinearity. The material GVD can be negative in the hypergap, because the sign of GVD flips across a resonance (the interband transition) where light slows down and the group velocity minimizes. In bandgap materials, such a transition is the optical phonon absorption at low energy, so the GVD can be negative in the infrared but turns positive again at optical frequencies. Interestingly, when the plasma frequency ($\omega_p$) locates inside a lossless hypergap, the negative GVD is divergent [GVD $\sim -(\omega - \omega_p)^{-3/2}$] toward the zero-epsilon[23] frequency, as we derive in Section SI (Supporting Information) and illustrate in Figure 1b. The large and negative material GVDs could be used to miniaturize ultrafast optical systems by replacing the bulky grating or prism pairs with hypergap materials.

Inspired by the above exciting opportunities in hypergaps, we perform a high-throughput search in the material databases of all known inorganic materials and found over a hundred high-quality hypergap candidates with their optical properties calculated, tabulated, analyzed, and discussed. We then grow the crystal of one candidate and measure its optical constants to validate our theory.

## 2. Hypergap Criteria

The density of states (DOS) of electrons in a hypergap material is illustrated in Figure 1a, where both the conduction and valence bands are sufficiently isolated from the hyper-conduction and the hyper-valence bands. The optical transitions can take place either from the valence to the conduction bands (interband absorption), or from the valence/hyper-valence band to the hyper-conduction/conduction bands (hyper-interband absorption). What separates these two absorptive regions is the hypergap, shown in Figure 1b, which can be identified from the vanishing joint DOS (JDOS). Different from the JDOS requiring momentum conservation, we relaxed it[14] to account for the indirect transitions assisted by phonons or imperfections.

The criteria for the hypergap, of bandwidth $\Delta\omega$, is

$$\hbar\Delta\omega = \min\{G_c, G_v\} - W > 0 \tag{1}$$

where $W$ is the lower-edge energy of the hypergap, from the bottom of the valence band to the top of the conduction band. The upper-edge energy of the hypergap is defined by the minimal value between $G_c$ and $G_v$, which are the gaps from the top of the valence/hyper-valence band to the bottom of the hyper-conduction/conduction band. When the bandgap $E_g$ shrinks to zero, the solid becomes the hypergap transparent conductor[24,25] that was reported recently. We focus on the hypergap insulators in this work, which are more promising experimentally.

## 3. High-Throughput Search

We search for hypergap materials in two major computational material databases of Materials Project (materialsproject.org) and AFLOW (aflow.org), totaling around 200,000 entries (in September 2020). In order to find realistic candidates, we target the entries whose structure data is from the Inorganic Crystal Structure Database (ICSD, icsd.fiz-karlsruhe.de), a comprehensive collection of experimental crystal data. After removing the metals with zero bandgaps[14] and combining the redundant entries of identical stoichiometries and space groups, we start with 23334 insulating band structures of magnetic or nonmagnetic ground states, as shown in **Figure 2a**.

In this search, we focus on the potential nonmagnetic material properties, which we screen with the density-functional theory (DFT), because the magnetic state usually appears at low temperatures and is challenging to predict. For the 18224 nonmagnetic spin-degenerate band structures, we keep the 1362 candidates that satisfy the hypergap criteria. For magnetic band structures, we separate the two spin bands and keep the 1098 candidates when either one of the spin bands satisfy the hypergap criteria. This criteria relaxation on spins is justified by the fact that magnetism mainly splits the energy difference between the two spin bands.

We perform non-magnetic recalculation for the above 2460 candidates, screened from the databases, whose computations trade accuracy for speed. In addition, we use the experimental lattice data from ICSD, instead of the numerically relaxed structures in the databases. The settings of the DFT calculations are provided in the Supporting Information. The hypergaps of 1466 candidates survive our recalculations, but 534 of them turn into "metals" whose bandgap closes. We do not consider these hypergap metals further here, because we have already done a high-throughput search for these hypergap (lossless) metals in Ref. [14], whose results suggest that simple DFT is not reliable to predict narrow-band metals for experiments. Therefore, 932 hypergap insulators remain and are tabulated in the Supporting Information Excel file.

To select the large-gap candidates with potentially lower optical losses, we set a lower bound on the hypergap size that is $\hbar\Delta\omega > 0.5$ eV, because the wider the gap size, the lower the optical absorption, which is generally valid for bandgap materials. It is known that the absorption coefficient drops exponentially at the band-edge into the gap — the universal Urbach tail.[26,27] Similarly, the absorption in the hypergap should also be limited by the interband and hyper-interband absorption tails from both band edges. The 0.5 eV lower bound removes 711 out of the 932 candidates. We then calculate the dielectric constants for the remaining 221 candidates and classify their optical responses (examples in **Table 1**).

## 4. Hypergap Candidates

The above search shows that the abundance of hypergap materials could be a few percent among existing inorganic compounds. Among the 221 candidates that have all been experimentally synthesized in the literature, many are commercially available in their powder form, including $MIO_4$, $M_2NiF_6$, $M_2TeO_4$, $SeCl_4$, $MSbF_6$, $M_2PbCl_6$, and $Mo(CO)_6$, where $M$ = Na, K, Rb, Cs. However, the optical data of the candidates are largely unknown, especially at the wavelengths where the hypergaps are predicted.

Here we discuss the general features of the hypergap candidates, in Table 1, which are mostly multinary compounds of three, four, and five elements. The majority have fluorine and oxygen, forming strong ionic bonds with metal elements, responsible for the wide energy separation between the hyper-valence and hyper-conduction bands. Many of the isolated narrow conduction and valence bands consist of either the split $d/f$ orbitals of transition metals under the crystalline fields, or the $s/p$ orbitals in the unit cells enlarged by molecular clusters such as $CH_3$, $NH_3$, and $H_2O$. The $d/f$ bands are intrinsically more localized and the larger the unit cell the weaker the inter-atomic couplings – both mechanisms result in narrow bands.

The distribution of the hypergaps is plotted in Figure 2b according to their energies and bandwidths. The hypergaps cover a wide spectrum spanning from 0.1 to 10 eV, whose maximal bandwidth reaches 3.4 eV in solid ozone.[28] Since DFT is known to underestimate the bandgap energy, the hypergap energies (not bandwidth) should be higher in reality than the values reported here, as seen from the comparison to the state-of-the-art Bethe-Salpeter-equation (BSE) calculations in Supporting Information. Therefore, hypergap could be a new direction for finding transparent deep-ultraviolet optical materials,[29,30] offering alternatives to those having large bandgaps.

Negative permittivity is found in 39 candidates in their hypergaps, which is highlighted in red color in Figure 2b. In about half of these candidates, $\epsilon_1 < 0$ takes place in only one crystal direction (the hyperbolic materials)[31] due to the anisotropic lattices. We note that lossless negative permittivity means total reflection, which could be used to identify such materials through reflection measurements.

Anomalous-dispersion phase matching is found in 74 candidates. 13 noncentrosymmetric candidates support second-harmonic generation (SHG) and 73 candidates support third-harmonic generation (THG), whose harmonic energies are highlighted in green and blue dots in Figure 2b. We note that the predicted harmonic energy (>9 eV) in solid carbon monoxide[32] is larger than the bandgap (8.44 eV) of the deep-ultraviolet nonlinear crystal $KBe_2BO_3F_2$ (KBBF).[33,34] Hence, hypergap crystals could be a new route to generate ultraviolet light for lithography and spectroscopy.

Negative GVDs are found in 155 candidates shown in Figure 2c, where the averaged (negative) GVDs and their central frequencies are plotted as yellow dots. (We do not sample the narrow-band divergent region; the energy internal used is 0.027eV.) For comparison, the negative GVDs of common optical materials are plotted in black squares, with the experimental data collected from the online database (https://refractiveindex.info). It is evident, in Figure 2c, that only the hypergap can provide negative GVDs at the short wavelengths (<1μm) and the amplitudes of the GVDs in hypergaps are larger than those in bandgaps.

The remaining 53 out of the 221 candidates have none of the unconventional optical properties listed above, due to their weak interband transitions. When the interband absorption induces no noticeable anomalous dispersion, the optics within the two gaps behave no differently.

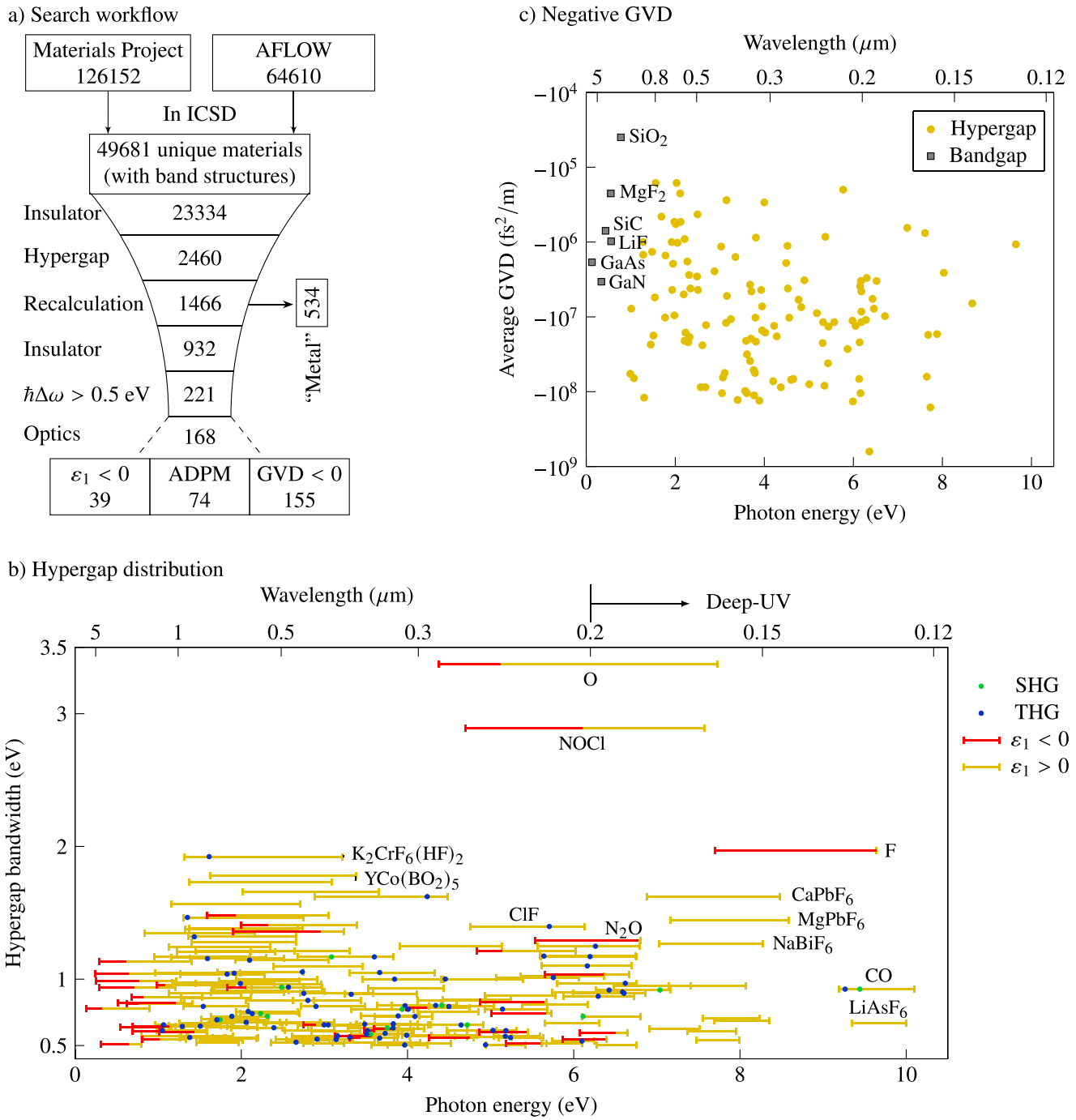


**Figure 2.** High-throughput screening results of hypergaps. a) The workflow of the high-throughput hypergap search from materials in the online databases. b) The energy distribution of the hypergaps in the candidates. The line segment is the energy interval of the hypergaps, in which the red section indicates negative permittivity ($\varepsilon_1 < 0$). The green and blue dots represent the energies of the second and third harmonics (SHG and THG) in the hypergaps that are anomalous-dispersion phase-matched. c) The averaged amplitudes and wavelengths of the negative GVDs of the hypergap materials in calculations. The black squares represent the averaged negative GVDs of bandgap materials in experiments.

## 5. Three Examples

To demonstrate the unusual optics inside the hypergap, we showcase three candidate ionic crystals of the cubic lattice in **Figure 3**, one in each category of Table 1.

Rubidium hexafluoroniccolate (IV) $Rb_2NiF_6$,[35] of space group 225 ($Fm\bar{3}m$) in Figure 3a, exhibits a negative dielectric constant ($\varepsilon_1 < 0$) in the hypergap. The isolated valence band and conduction band consist of Ni 3*d* and F 2*p* orbitals. $Rb_2NiF_6$ can be synthesized via fluorination of $Rb_2NiCl_4$.[36] The negative permit-

**Table 1.** High-quality hypergap candidates. $\delta\omega$ is the negative-permittivity ($\varepsilon_1$) bandwidth within the hypergap, and the lowest $\varepsilon_1$ values in the hypergaps are listed. The non-centrosymmetric space-group numbers are in bold, and $2\omega$ ($3\omega$) is the harmonic energy of SHG (THG). More details of each compound are tabulated in the Supporting Information.

| Categaries | Formula | Space group | $E_g$ [eV] | $W$ [eV] | $\hbar\Delta\omega$ [eV] | Optical properties |
|---|---|---|---|---|---|---|
| Low-loss negative permittivity for nano-optics | $CuAlAsO_5$ | 14 | 0.34 | 0.68 | 0.64 | $\varepsilon_1 = -27.87$, $\delta\omega = 0.45$ eV |
| | $Cs_6Cr_2O_7$ | 14 | 0.11 | 0.30 | 0.51 | $\varepsilon_1 = -23.33$, $\delta\omega = 0.35$ eV |
| | $Cs_4U_3Si_4O_{17}$ | 12 | 0.52 | 0.68 | 0.61 | $\varepsilon_1 = -16.88$, $\delta\omega = 0.34$ eV |
| | $KHC(NO)_2$ | **122** | 0.78 | 1.89 | 1.36 | $\varepsilon_1 = -12.33$, $\delta\omega = 1.06$ eV |
| | $B_{20}H_{26}O$ | 15 | 0.41 | 1.00 | 0.60 | $\varepsilon_1 = -9.66$, $\delta\omega = 0.44$ eV |
| | $Rb_2NiF_6$ | 225 | 2.30 | 6.90 | 0.62 | $\varepsilon_1 = -8.70$, $\delta\omega = 0.66$ eV |
| | $H_3CBrClF$ | 62 | 1.57 | 3.11 | 0.57 | $\varepsilon_1 = -8.39$, $\delta\omega = 0.46$ eV |
| | $Mo(CO)_6$ | 62 | 3.67 | 4.86 | 0.83 | $\varepsilon_1 = -8.36$, $\delta\omega = 0.79$ eV |
| | $F_2$ | 15 | 1.37 | 7.68 | 1.97 | $\varepsilon_1 = -7.98$, $\delta\omega = 1.96$ eV |
| Anomalous-dispersion phase matching for nonlinear optics | $CsIO_4$ | 62 | 3.16 | 5.56 | 1.25 | $3\omega = 6.26$ eV |
| | $NH_2TeF_5$ | **4** | 1.95 | 2.67 | 1.17 | $2\omega = 3.09$ eV, $3\omega = 3.60$ eV |
| | $LiVP_2O_7$ | **4** | 1.54 | 2.04 | 0.94 | $2\omega = 2.48$ eV, $3\omega = 2.57$ eV |
| | $[C(NH_2)_3][N(CH_3)_4]CrO_4$ | **198** | 3.55 | 3.80 | 0.80 | $2\omega = 4.41$ eV, $3\omega = 4.34$ eV |
| | $GaNO_2(NO_3)_4$ | **82** | 1.60 | 1.97 | 0.74 | $2\omega = 2.23$ eV, $3\omega = 2.13$ eV |
| | $Zn(NH_3)_4(MnO_4)_2$ | **216** | 1.50 | 1.63 | 0.69 | $2\omega = 1.75$ eV, $3\omega = 1.71$ eV |
| | $N_2H_5HSO_4$ | **19** | 2.32 | 5.64 | 0.67 | $2\omega = 3.92$ eV, $3\omega = 3.99$ eV |
| | $ZrH_{16}C_5N_2O_3F_4$ | **41** | 4.01 | 4.27 | 0.66 | $2\omega = 4.72$ eV, $3\omega = 4.64$ eV |
| | $MoH_{12}N_3O_5F_3$ | **19** | 2.71 | 3.27 | 0.63 | $2\omega = 3.75$ eV, $3\omega = 3.83$ eV |
| | $K_3NaUC_3O_{11}$ | **190** | 3.10 | 3.31 | 0.58 | $2\omega = 3.56$ eV, $3\omega = 3.51$ eV |
| Negative GVD for ultrafast optics | $Cs_2PdF_6$ | 225 | 3.08 | 6.06 | 0.60 | GVD= $-6.36\times10^8$ fs$^2$/m |
| | $NaSbF_6$ | 205 | 3.24 | 7.46 | 0.54 | GVD= $-1.64\times10^8$ fs$^2$/m |
| | $B_4COF_6$ | 14 | 5.16 | 5.73 | 0.53 | GVD= $-1.34\times10^8$ fs$^2$/m |
| | $C_2N$ | 205 | 3.19 | 3.58 | 0.62 | GVD= $-1.32\times10^8$ fs$^2$/m |
| | $AgKF_4$ | 140 | 2.98 | 5.64 | 1.04 | GVD= $-1.05\times10^8$ fs$^2$/m |
| | $K_2SN_2O_5$ | 62 | 2.88 | 4.27 | 0.58 | GVD= $-9.72\times10^7$ fs$^2$/m |
| | $CsBrF_6$ | 148 | 4.26 | 4.92 | 0.87 | GVD= $-8.25\times10^7$ fs$^2$/m |
| | $CsCa(NO_2)_3$ | **146** | 2.67 | 5.35 | 1.02 | GVD= $-2.71\times10^7$ fs$^2$/m |
| | $CaPbF_6$ | 225 | 3.16 | 6.87 | 1.62 | GVD= $-1.73\times10^7$ fs$^2$/m |
| | $Cs_2TeO_4$ | 62 | 3.05 | 5.06 | 1.01 | GVD= $-1.18\times10^7$ fs$^2$/m |

tivity in the hypergap could support low-loss surface-plasmon-polariton (SPP), whose dispersion is plotted in Figure 3a4. The hypergap, including the hypergap metal,[13,14,25] is so far the only proposed mechanism for near-lossless SPP, important for ultra-compact optical devices and extreme light-matter interactions.

Tetramethylammonium guanidinium chromate[37] $[C(NH_2)_3][N(CH_3)_4]CrO_4$ of space group 198 ($P2_13$), in Figure 3b, supports anomalous-dispersion phase matching for both SHG (281 nm) and THG (286 nm) inside the hypergap ranging from 3.8 eV to 4.6 eV. The presence of the cation groups $[N(CH_3)_4]^+$ and $[C(NH_2)_3]^+$ enlarge the unit cell, resulting in the isolated flat bands made of the Cr $3d$ and O $2p$ orbitals in the $[CrO_4]^{2-}$ anion group. Large negative GVD is also predicted in the hypergap.

Calcium hexafluoroplumbate $CaPbF_6$,[38] of space group 225 ($Fm\bar{3}m$) in Figure 3c, is predicted to have negative GVD in the hypergap. The isolated conduction and valence bands consist of the $p$ orbitals from the F and the $s$ orbitals from the Pb atoms, in the anion group $[PbF_6]^{2-}$. $CaPbF_6$ can be synthesized via a solid-state fluorination reaction, where stoichiometric amounts of $CaCO_3$ and PbO are reacted under a continuous flow of $F_2$ gas at 420°C. A transparent hypergap material of negative GVD could be used in dispersion management of short pulses, in which the required anomalous dispersion is not generally available in the bandgap at optical wavelengths.

## 6. Experimental Verification

To verify this proposal and prediction, the $[C(NH_2)_3][N(CH_3)_4]CrO_4$ crystal in Figure 3 was grown and characterized, as it simultaneously possesses two unique hypergap properties: anomalous-dispersion phase matching and negative GVD. The single crystal[37] was synthesized via a solution growth method. Potassium chromate $K_2CrO_4$ serves as the source of chromate anions, while guanidinium chloride $CH_6ClN_3$ and tetramethylammonium chloride $(CH_3)_4NCl$ provide the organic cations. These components were dissolved in hot (60°C) deionized water to form a clear solution. Hot (60°C) dimethyl sulfoxide DMSO was then added as a co-solvent to improve the solubility of the organic components. Upon

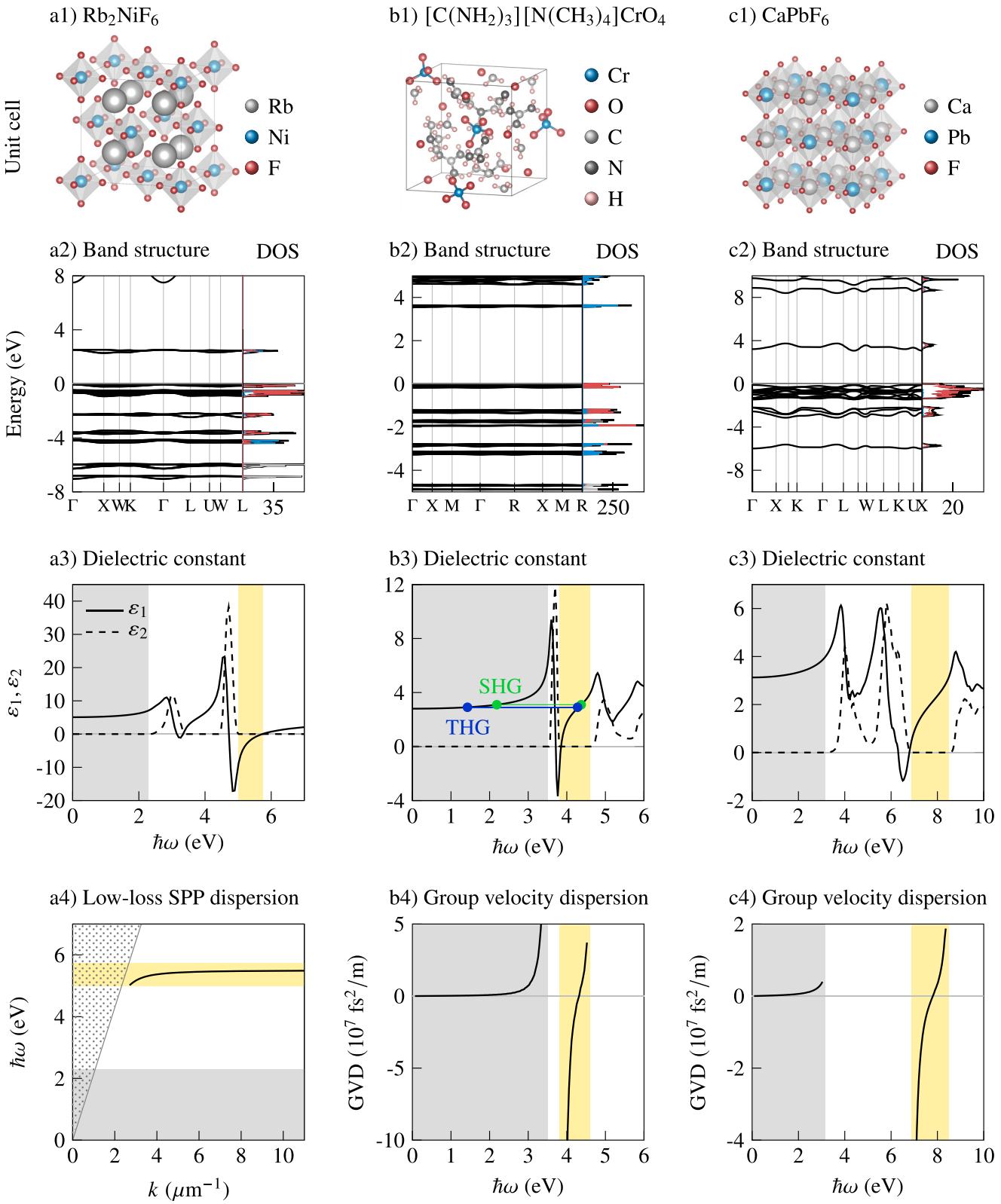


**Figure 3.** Examples of ionic hypergap materials of cubic lattice. The crystal structure, band structure and dielectric constant of a1–a3) Rubidium hexafluoroniccolate (IV) $Rb_2NiF_6$, b1–b3) Tetramethylammonium guanidinium chromate $[C(NH_2)_3][N(CH_3)_4]CrO_4$, and c1–c3) calcium hexafluoroplumbate $CaPbF_6$. a4) The dispersion of low-loss surface plasmon polariton (SPP) in the hypergap, where the dotted triangular area is the light cone. b4, c4) The group velocity dispersions in the bandgaps and hypergaps. We also supply their dielectric functions computed with BSE methods in the Supporting Information.

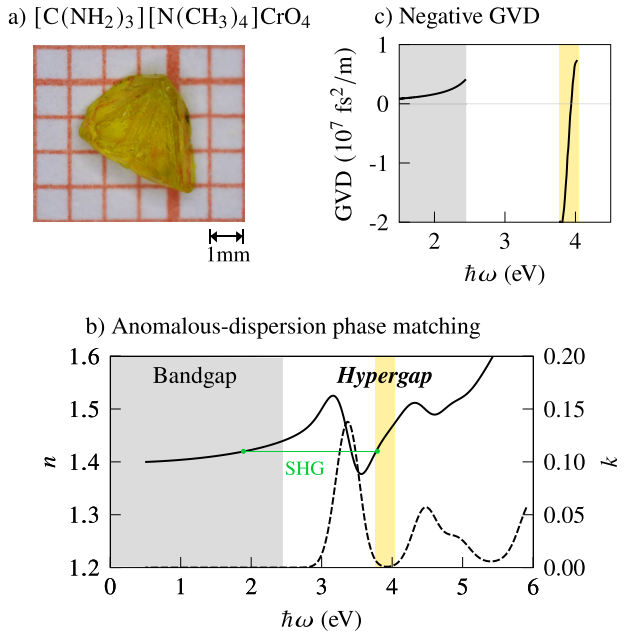


**Figure 4.** Experiments on a hypergap candidate. a) Crystal sample of tetramethylammonium guanidinium chromate. b) The refractive index from ellipsometry showing anomalous-dispersion phase matching for SHG. c) Negative GVD in the hypergap.

slow cooling to room temperature, bright yellow crystals were obtained, as shown in **Figure** 4a.

The presence of the hypergap, the anomalous-dispersion phase matching, and the negative GVD were demonstrated through the optical constants in Figure 4b,c. The refractive index ($n$) and the extinction coefficient ($k$) of the crystal were measured using a spectroscopic ellipsometry (J.A Woollam RC2-XI) with photon energy from 0.5 to 5.9 eV. The $k$ spectrum exhibits vanishing values at two spectrum ranges as predicted by the high-throughput search in Table 1. One low-loss range was the bandgap below 2.45 eV, and the second low-loss range was the hypergap from 3.77 to 4.04 eV. In the hypergap, the $n$ value matches that in the bandgap, for SHG at 3.78 eV (328 nm), enabled by the anomalous dispersion due to the interband absorption between the two gaps. The matching wavelength for THG was outside of the hypergap. Furthermore, the GVD = $\frac{1}{c}(2\frac{dn}{d\omega} + \omega\frac{d^2n}{d\omega^2})$, in Figure 4c, were indeed negative inside the hypergap of $[C(NH_2)_3][N(CH_3)_4]CrO_4$. The follow-up experiments on the anomalous-dispersion phase-matched THG generation in $K_2CrO_4$ are reported in ref. [41].

## 7. Discussion

The experimental demonstration, of two anomalous optical properties in the predicted hypergap candidate, show the viability of our proposal and approach. As seen by comparing the calculations in Figure 3b and measurements in Figure 4, the qualitative behaviors agree well. In general, however, the quantitative values predicted in this work should be interpreted with caution, due to the limitations of the high-throughput DFT methods. For further reference, we apply the state-of-the-art many-body perturbation theory (BSE) to the other two example materials in the Supporting Information.

The optics in the hypergap are determined by both the interband and hyper-interband transitions, the two absorption peaks sandwiching the hypergap are illustrated in Figure 1b. The strong interband transition, inducing the anomalous dispersion, is necessary for all three unusual optical properties in the hypergap. (It could equally induce a high refractive index in the bandgap).[39,40] This distinguishes the hypergap materials from the other material systems with similar DOS distributions. For example, the defect states in bandgap materials or the dye molecules in transparent liquids can introduce isolated states as in Figure 1a, but their DOS will be too low to generate sufficient absorption and anomalous dispersions.

Our current search is nowhere near complete. We have not investigated the potential hypergap materials with magnetic ground states, while they often occur in narrow-band systems under low temperatures. Although the candidates of hypergap metals in ref. [14] and this work are predominantly false metals, some of them could be hypergap (Hubbard) insulators if the hypergap persists. The search for hypergap materials should be extended to organic compounds. Moreover, a hypergap may emerge between the exciton peak and the bandedge, provided that the exciton binding energy is large enough to separate its absorption from the bandedge absorption.

## 8. Conclusion

We show that there are plenty of opportunities in novel optical materials when one looks beyond the fundamental bandgaps into the new low-loss regions of the proposed hypergaps. These hypergap dielectrics could exhibit unprecedented optical properties, such as negative permittivity, anomalous-dispersion phase matching, and negative GVD, promoting the paradigm shifts in plasmonics, nonlinear optics, and ultrafast optics. Among all existing inorganic materials, we identify 221 hypergap candidates whose syntheses and characterizations can be readily performed and are highly encouraged, as we have done for $[C(NH_2)_3][N(CH_3)_4]CrO_4$. The eventual discovery of hypergap materials with low enough absorption coefficients could impact many areas of optics.

## Supporting Information

Supporting Information is available from the Wiley Online Library or from the author.

## Acknowledgements

The authors thank Guoqing Chang, Yuen-Ron Shen, Bei Tang, and Xinguo Ren for discussions. This work was supported by the Natural Science Foundation of China (12025409), and by the Chinese Academy of Sciences through the Project for Young Scientists in Basic Research (YSBR-021), through the Youth Innovation Promotion Association (No. 2021008), and through the IOP-HKUST-Joint Laboratory for Wave Functional Materials Research.

## Conflict of Interest

The authors declare no conflict of interest.

## Data Availability Statement

The data that support the findings of this study are available in the supplementary material of this article.

## Keywords

DFT calculations, high-throughput search, optical materials

Received: July 7, 2025
Published online: October 3, 2025

[1] E. D. Palik, *Handbook of optical constants of solids*, Vol. *3*, Academic press, Cambridge, **1998**.
[2] M. J. Weber, *Handbook of optical materials*, Vol. *19*, CRC press, Boca Raton, **2002**.
[3] M. Fox, *Optical Properties of Solids*, Vol. *3*, Oxford University Press, Oxford, **2010**.
[4] V. G. Dmitriev, G. G. Gurzadyan, D. N. Nikogosyan, *Handbook of nonlinear optical crystals*, Vol. *64*, Springer, Berlin, **2013**.
[5] W. Cai, V. M. Shalaev, *Optical metamaterials*, Vol. *10*, Springer, Berlin, **2010**.
[6] A. Boltasseva, H. A. Atwater, *Science* **2011**, *331*, 290.
[7] Y.-R. Shen, *Principles of nonlinear optics*, Wiley-Interscience, New York, NY, USA, **1984**.
[8] R. W. Boyd, *Nonlinear optics*, Academic press, Cambridge, **2020**.
[9] A. Weiner, *Ultrafast optics*, Vol. *72*, John Wiley & Sons, New York, **2011**.
[10] U. Keller, R. Paschotta, *Ultrafast Lasers*, Springer, Berlin, **2021**.
[11] J. B. Khurgin, *Nat. Nanotechnol.* **2015**, *10*, 2.
[12] G. V. Naik, V. M. Shalaev, A. Boltasseva, *Adv. Mater.* **2013**, *25*, 3264.
[13] J. B. Khurgin, G. Sun, *Appl. Phys. Lett.* **2010**, *96*, 181102.
[14] X. Hu, Z. Wu, Z. Li, Q. Xu, K. Chen, W. Hu, Z. Ni, K. Jin, H. Weng, L. Lu, *Phys. Rev. Mater.* **2022**, *6*, 065203.
[15] M. N. Gjerding, M. Pandey, K. S. Thygesen, *Nat. Commun.* **2017**, *8*, 15133.
[16] P. P. Bey, J. F. Giuliani, H. Rabin, *Phys. Rev. Lett.* **1967**, *19*, 819.
[17] J. F. Young, G. Bjorklund, A. Kung, R. Miles, S. Harris, *Phys. Rev. Lett.* **1971**, *27*, 1551.
[18] T. Kowalczyk, K. Singer, P. Cahill, *Opt. Lett.* **1995**, *20*, 2273.
[19] M. T. Anderson, M. L. Phillips, G. D. Stucky, *J. Non-Cryst. Solids* **1994**, *178*, 120.
[20] J. P. Torres, M. Hendrych, A. Valencia, *Adv. Opt. Photonics* **2010**, *2*, 319.
[21] E. Treacy, *IEEE J. Quantum Electron.* **1969**, *5*, 454.
[22] R. Fork, O. Martinez, J. Gordon, *Opt. Lett.* **1984**, *9*, 150.
[23] O. Reshef, I. De Leon, M. Z. Alam, R. W. Boyd, *Nat. Rev. Mater.* **2019**, *4*, 535.
[24] J. E. Medvedeva, A. J. Freeman, *EPL (Europhysics Lett.)* **2005**, *69*, 583.
[25] Z. Wu, C. Li, X. Hu, K. Chen, X. Guo, Y. Li, L. Lu, *Nat. Mater.* **2025**, *24*, 1387.
[26] F. Urbach, *Phys. Rev.* **1953**, *92*, 1324.
[27] M. Grundmann, *Physics of Semiconductors*, Springer, Berlin, **2010**.
[28] R. Marx, R. M. Ibberson, *Solid State Sci.* **2001**, *3*, 195.
[29] T. T. Tran, H. Yu, J. M. Rondinelli, K. R. Poeppelmeier, P. S. Halasyamani, *Chem. Mater.* **2016**, *28*, 5238.
[30] D. Ehrt, *Adv. Opt. Technol.* **2018**, *7*, 225.
[31] K. Korzeb, M. Gajc, D. A. Pawlak, *Opt. Express* **2015**, *23*, 25406.
[32] I. Vegard, *Z. Phys.* **1930**, *61*, 185.
[33] T. Nakazato, I. Ito, Y. Kobayashi, X. Wang, C. Chen, S. Watanabe, *Opt. Express* **2016**, *24*, 17149.
[34] C. Chen, T. Sasaki, R. Li, Y. Wu, Z. Lin, Y. Mori, Z. Hu, J. Wang, G. Aka, M. Yoshimura, Y. Kaneda, *Nonlinear optical borate crystals: Principals and applications*, John Wiley & Sons, New York, **2012**.
[35] M. G. Brik, M. Piasecki, N. M. Avram, *Phys. Status Solidi (b)* **2022**, *259*, 2100607.
[36] H. Bode, E. Voss, *Z. Anorg. Allg. Chem.* **1956**, *286*, 136.
[37] B. F. Abrahams, M. G. Haywood, T. A. Hudson, R. Robson, *Angew. Chem., Int. Ed.* **2004**, *43*, 6157.
[38] R. Hoppe, K. Blinne, *Z. Anorg. Allg. Chem.* **1958**, *293*, 251.
[39] H. Shim, F. Monticone, O. D. Miller, *Adv. Mater.* **2021**, *33*, 2103946.
[40] J. B. Khurgin, *Acs Photonics* **2022**, *9*, 743.
[41] K. Chen, X. Hu, Z. Wu, X. Guo, Z. Li, L. Lu, *Phys. Rev. A* **2025**, https://doi.org/10.1103/hnf1-vj2r.